

Supporting Information

Facile One-Pot Synthesis of Highly Monodisperse Nickel Microspheres with Raised Nickel Dots and Their Adsorption Performance for Heavy Metal Ions

Yue Teng^a, Le Xin Song^{a,b,*}, Wei Liu^{a,*}, Li Zhao^b, Juan Xia^c, Qing Shan Wang^b, Mao Mao Ruan^b, Zun Yang^b and Yong Xin Qian^b

^a CAS Key Laboratory of Materials for Energy Conversion & Collaborative Innovation Center of Suzhou Nano Science and Technology, University of Science and Technology of China, Jin Zhai Road 96, Hefei, China 230026, E-mail: wliu@ustc.edu.cn;.

^b Department of Chemistry, University of Science and Technology of China, Jin Zhai Road 96, Hefei 230026, China. E-mail: solexin@ustc.edu.cn; Fax: +86-551-63601592;

^c School of Chemistry and Chemical Engineering, Fuyang Normal College, Fuyang Anhui 236037, China.

A list of the contents for all the supporting information

Pages	Contents
1	A table of contents page.
2	Fig. S1 The size distribution of the Ni microspheres.
3	Fig. S2 XRD patterns (A) of the Ni materials obtained from solvothermal processes at 10 (a), 15 (b), 18 (c) and 20 h (d); SEM images of the Ni materials obtained from solvothermal processes at 10 (B), 15 (C), 18 (D) and 20 h (E).
4	Fig. S3 (A) XRD patterns of the solvothermal products when the molar ratio of NATH to urea is 1:2 (a), 1:1 (b) and 2.5:1 (c); (B, C, D) SEM images of the solvothermal products when the molar ratio of NATH to urea is 1:2 (B), 1:1 (C) and 2.5:1 (D).
5	Fig. S4 (A) XRD patterns of the solvothermal products when the molar ratio of NATH to urea is 1:0 (a) and 3:1 (b); (B, C) SEM images of the solvothermal products when the molar ratio of NATH to urea is 1:0 (B) and 3:1 (C). The green asterisks represent the formation of the Ni-EG.
6	Fig. S5 The XRD pattern of the solvothermal product when the molar ratio of NaOH to urea is 2:1. The green asterisks represent the formation of the Ni-EG.
7	Fig. S6 The XRD pattern of the solvothermal products when the reaction temperature is 413 K. The green asterisks represent the formation of the Ni-EG.
8	Fig. S7 The XRD pattern of the solvothermal product when the reaction temperature is 433 K. The green asterisks represent the formation of the Ni-EG.
9	Fig. S8 The XRD pattern and SEM image of the solvothermal product when the reaction temperature is 473 K.
10	Table S1. Comparison of magnetic properties of the Ni microspheres with other Ni materials in literature.
11	Fig. S9 Temperature dependence of magnetization for the Ni microspheres. The curve was recorded at 100 Oe.
12	Fig. S10 The N ₂ adsorption-desorption isotherm and pore size distribution of the Ni microspheres.
13	Table S2. Comparison of adsorption activity of different materials for removal of Cd ²⁺ .
14	Fig. S11 EDS images of the Ni microspheres after adsorption of Cd ²⁺ (C ₀ , 3000 mg·L ⁻¹).
15	Fig. S12 Schematic drawing describing the proposed coordination bridging adsorption process of Cd ²⁺ ions on the Ni microspheres.
16	Fig. S13 The adsorption isotherm of Cd ²⁺ ions on the Ni microspheres (0.5 g·L ⁻¹) using Cd(NO ₃) ₂ instead of CdCl ₂ .
17	Fig. S14 Ni 2p _{1/2} and 2p _{3/2} , Cd 3d _{3/2} and 3d _{5/2} and Cl 2p _{1/2} and 2p _{3/2} XPS spectra on the Ni microspheres after adsorption treatment.
18	Fig. S15 The adsorption isotherm of Cd ²⁺ ions on the Ni microspheres (0.5 g·L ⁻¹ , red line) and a Ni material with a low density of Ni dots (0.5 g·L ⁻¹ , black line).
19	Fig. S16 The adsorption isotherm of Zn ²⁺ ions on the Ni microspheres (0.5 g·L ⁻¹) using ZnCl ₂ .
20	Fig. S17 The adsorption isotherm of Hg ²⁺ ions on the Ni microspheres (0.5 g·L ⁻¹) using HgCl ₂ .

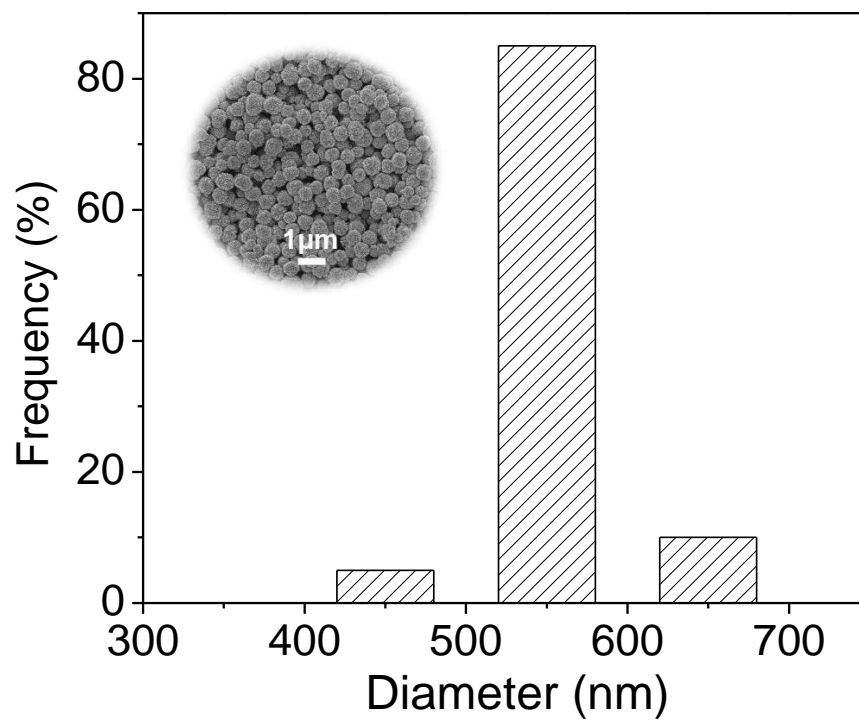


Fig. S1 The size distribution of the Ni microspheres (about 180 particles were measured and counted in the inset).

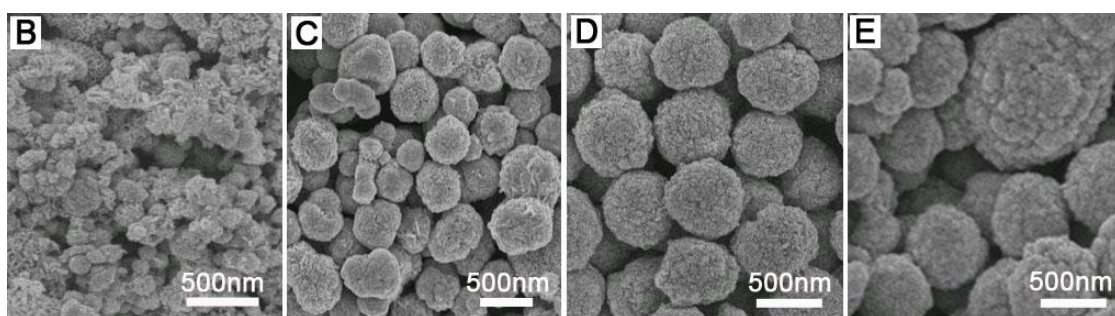
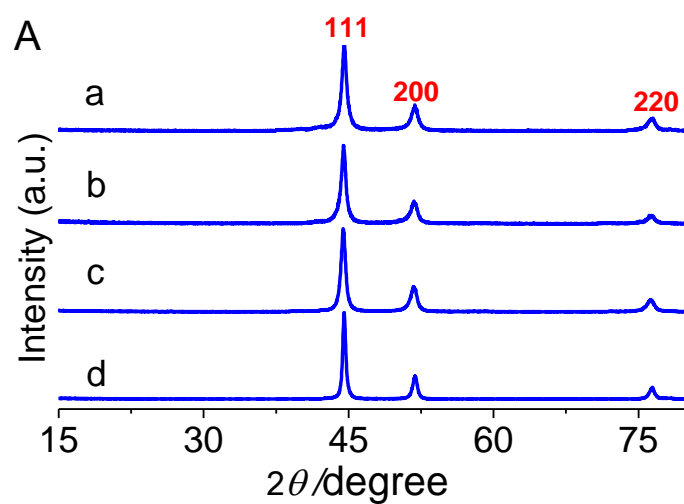


Fig. S2 XRD patterns (A) of the Ni materials obtained from solvothermal processes at 10 (a), 15 (b), 18 (c) and 20 h (d); SEM images of the Ni materials obtained from solvothermal processes at 10 (B), 15 (C), 18 (D) and 20 h (E).

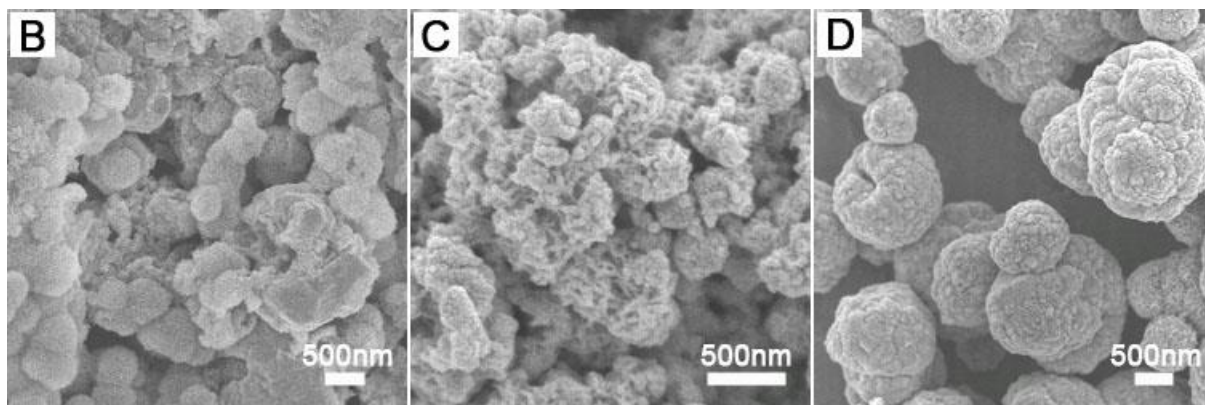
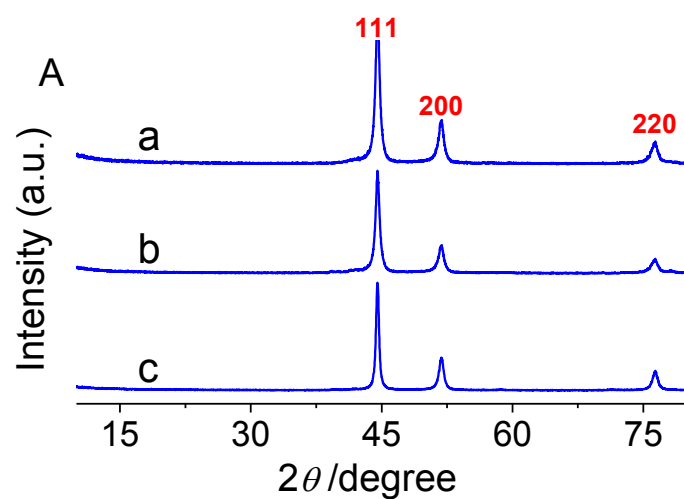


Fig. S3 (A) XRD patterns of the solvothermal products when the molar ratio of NATH to urea is 1:2 (a), 1:1 (b) and 2.5:1 (c); (B, C, D) SEM images of the solvothermal products when the molar ratio of NATH to urea is 1:2 (B), 1:1 (C) and 2.5:1 (D).

The X-ray diffraction (XRD) in **Fig. S4** shows that the products, obtained with the 1:0 and 3:1 initial molar ratios of NATH to urea, have a strong characteristic peak at around 10° and several small peaks, which were marked with green asterisks. These peaks do not belong to the characteristic peaks of Ni, but they can be indexed to pure Ni-EG complex according to the results reported before.^{1,2} This observation indicated that some Ni^{2+} ions were reacted with EG to form Ni-EG and the complex coexisted in the two samples of Ni.

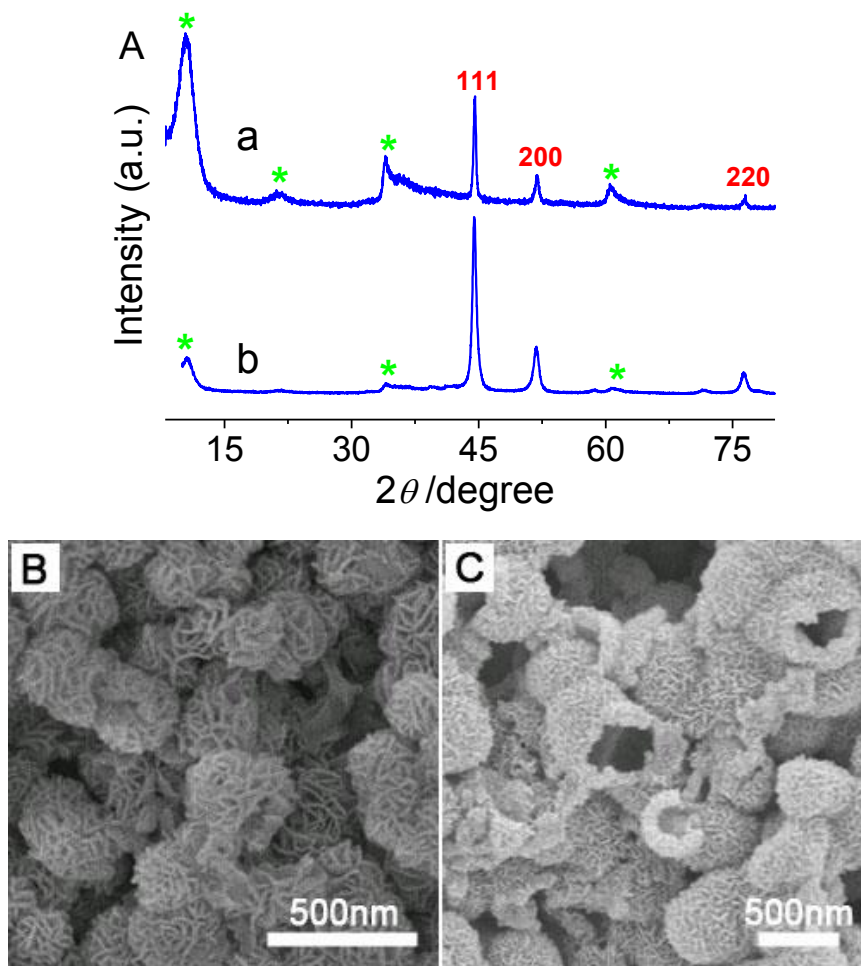


Fig. S4 (A) XRD patterns of the solvothermal products when the molar ratio of NATH to urea is 1:0 (a) and 3:1 (b); (B, C) SEM images of the solvothermal products when the molar ratio of NATH to urea is 1:0 (B) and 3:1 (C). The green asterisks represent the formation of the Ni-EG.

Reference

- (a) D. Khushalani, O. Dag, G. A. Ozin and A. Kuperman, *J. Mater. Chem.*, 1999, **9**, 1491. (b) F. F. Tao, M. Y. Guan, Y. M. Zhou, L. Zhang, Z. Xu and J. Chen, *Cryst. Growth Des.*, 2008, **8**, 2157. (c) L. S. Zhong, J. S. Hu, H. P. Liang, A. M. Cao, W. G. Song and L. J. Wan, *Adv. Mater.*, 2006, **18**, 2426.
- (a) X. C. Jiang, Y. L. Wang, T. Herricks and Y. N. Xia, *J. Mater. Chem.*, 2004, **14**, 695. (b) Y. L. Wang, X. C. Jiang and Y. N. Xia, *J. Am. Chem. Soc.*, 2003, **125**, 16176. (c) R. W. J. Scott, N. Coombs, L. J. Wan and G. A. Ozin, *J. Mater. Chem.*, 2003, **13**, 969.

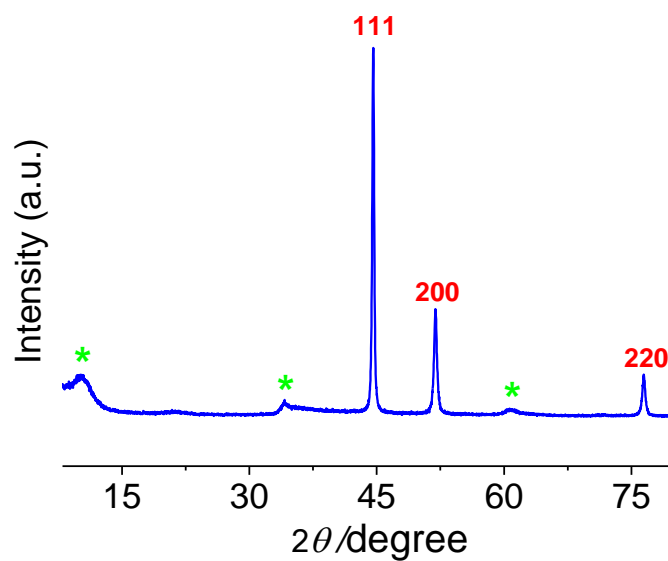


Fig. S5 The XRD pattern of the solvothermal product when the molar ratio of NaOH to urea is 2:1. The green asterisks represent the formation of the Ni-EG.

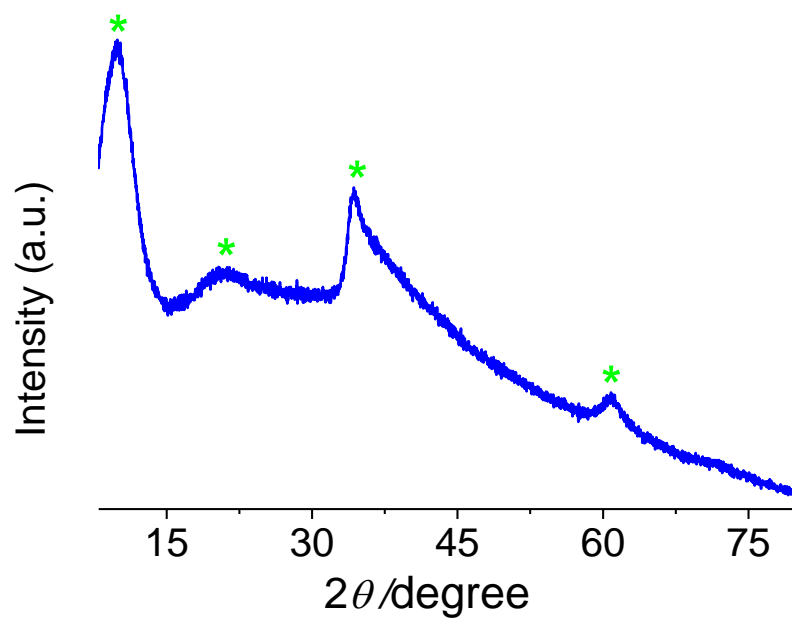


Fig. S6 The XRD pattern of the solvothermal product when the reaction temperature is 413 K. The green asterisks represent the formation of the Ni-EG.

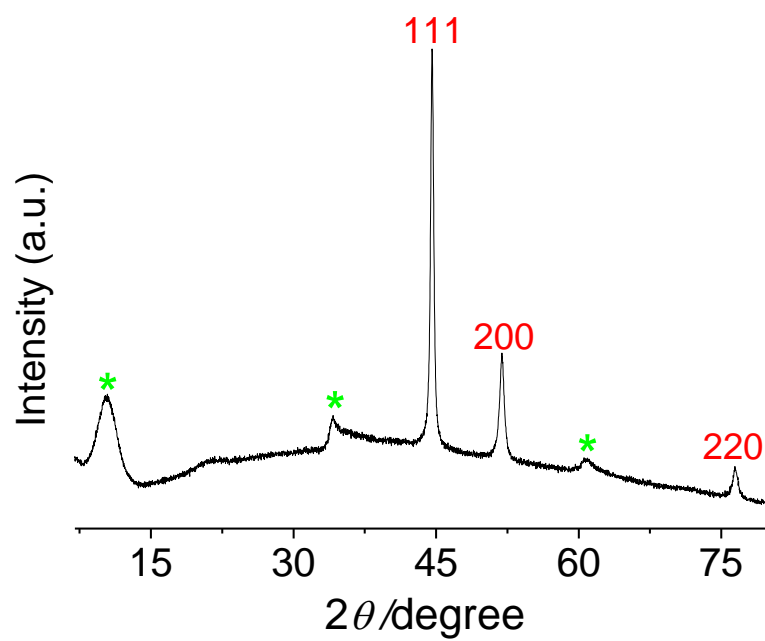


Fig. S7 The XRD pattern of the solvothermal product when the reaction temperature is 433 K. The green asterisks represent the formation of the Ni-EG.

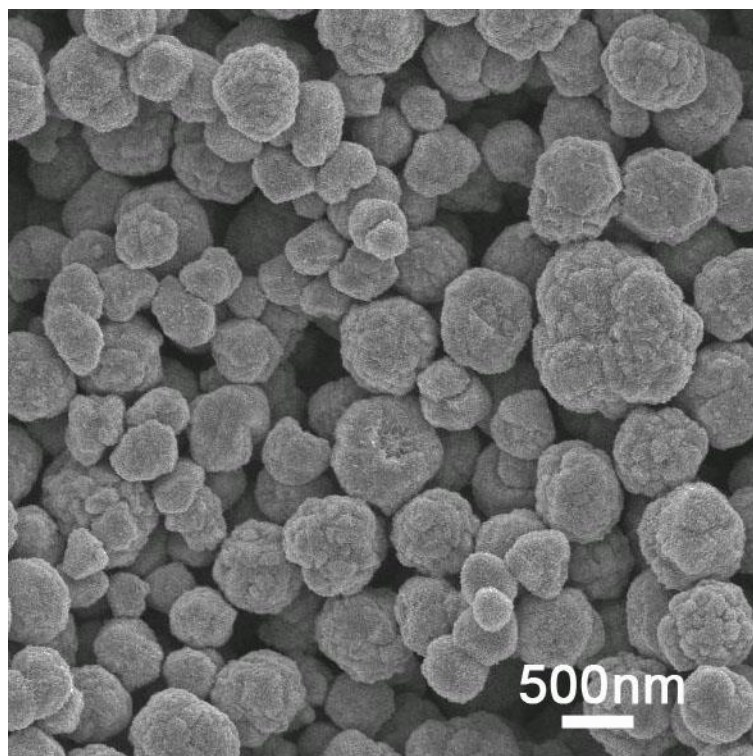
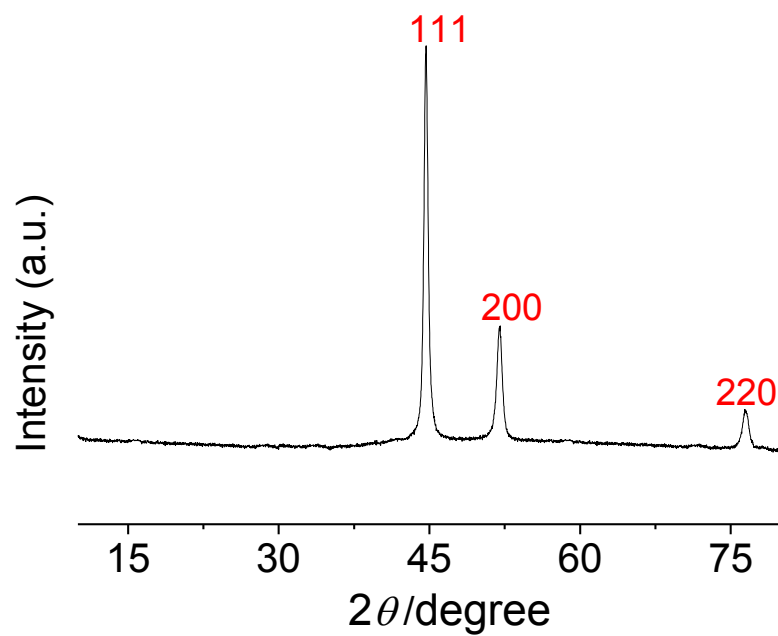


Fig. S8 The XRD pattern and SEM image of the solvothermal product when the reaction temperature is 473 K.

Table S1. Comparison of magnetic properties of the Ni microspheres with other Ni materials in literature.

Materials	Size (nm)	Saturation magnetization (emu·g ⁻¹)	Remnant Magnetization (emu·g ⁻¹)	Coercivity Values (Oe)	Temperature (K)	Reference
Ni microspheres	550	35.8	13.6	244	5	The present work
	550	40.4	4.2	90	300	
hollow Ni spheres	300-450	21.1	0.69	32.3	300	3
Ni@C honeycomb like nanostructures	500	13	/	124.2	300	4
bulk Ni	2000-3000	55	2.7	0.7	300	5

Reference

3. J. C. Bao, Y. Y. Liang, Z. Xu, L. Si, *Adv. Mater.*, 2003, **15**, 1832.
4. Y. H. Ni, L. N. Jin, L. Zhang, J. M. Hong, *J. Mater. Chem.*, 2010, **20**, 6430.
5. J. C. Bao, C. Y. Tie, Z. Xu, Q. F. Zhou, D. Shen, Q. Ma, *Adv. Mater.*, 2001, **13**, 1631.

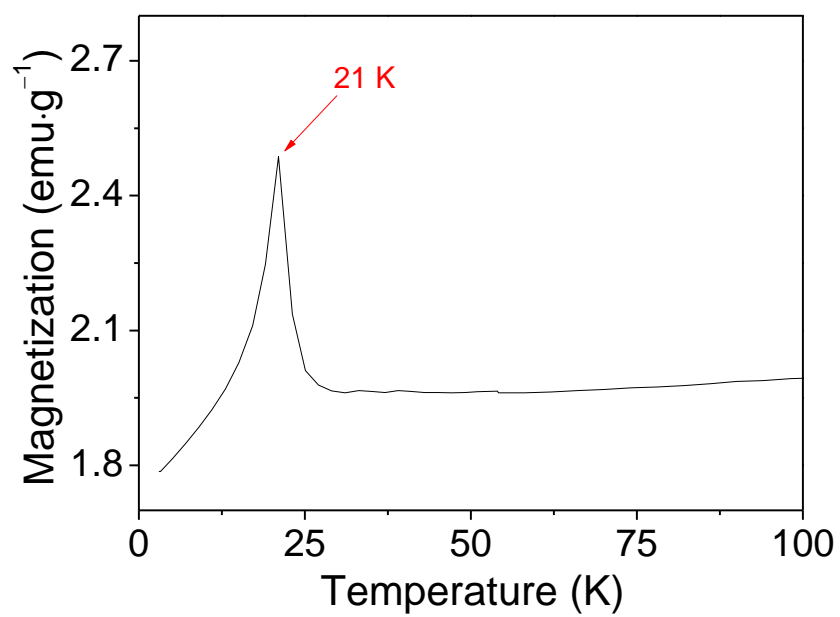


Fig. S9 The temperature dependence of magnetization for the Ni microspheres. The curve was recorded at 100 Oe.

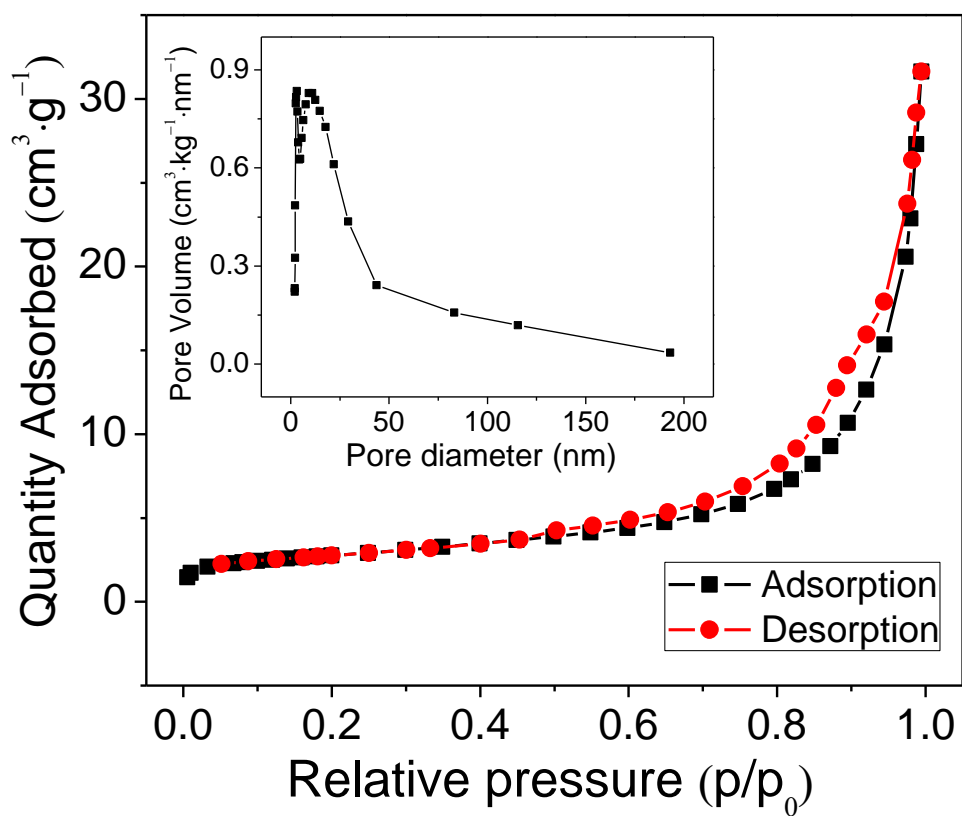


Fig. S10 The N_2 adsorption-desorption isotherm and pore size distribution of the Ni microspheres.

Table S2. Comparison of adsorption activity of different materials for removal of Cd²⁺.

Materials	Catalyst (mg)	C ₀ (Cd ²⁺ mg/L)	Volume (Cd ²⁺ /mL)	C _e (Cd ²⁺ /mL)	q _e (mg·g ⁻¹)	η (%)	Reference
Ni microspheres	10	12	20	3.86	16.28	68	The present work
	10	60	20	32.57	54.86	46	The present work
	10	600	20	100.00	1000.00	84	The present work
Ni-P microstructures	10	10	50	1.86	40.7	81.4	6
	10	50	50	28	110	44	6
Ni@C nanostructures	20	10	50	4.7	6.43	53	7

Reference

6. Y. H. Ni, K. Mi, C. Cheng, J. Xia, X. Ma, J. M. Hong, *Chem. Commun.* 2011, **47**, 5891.
7. Y. Ni, L. Jin, L. Zhang and J. Hong, *J. Mater. Chem.*, 2010, **20**, 6430.

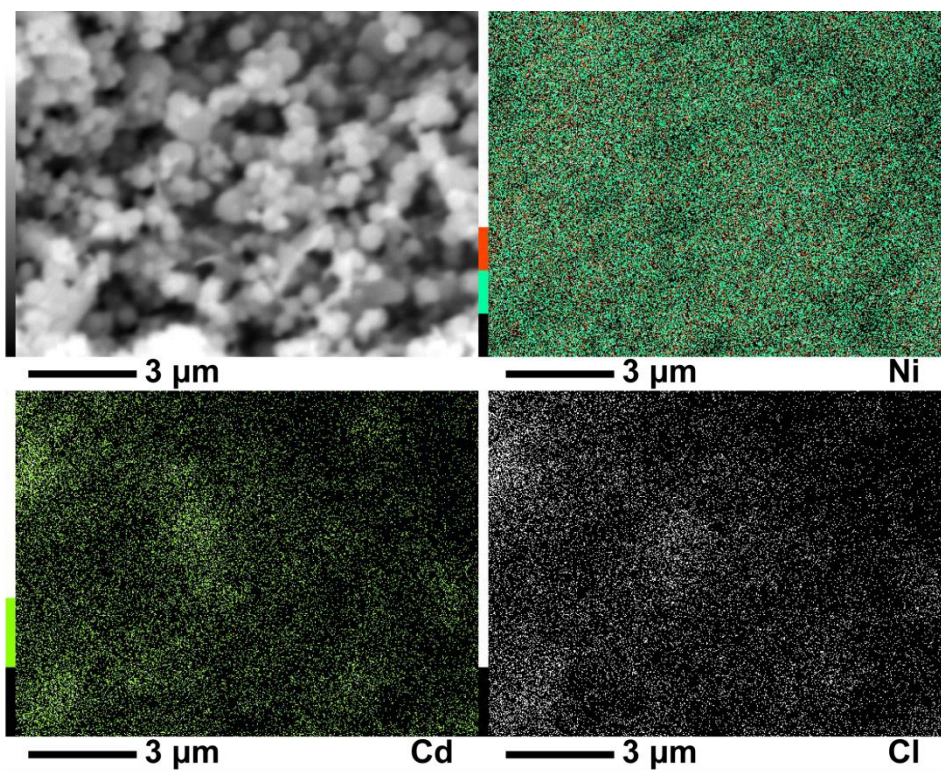


Fig. S11 EDS images of the Ni microspheres after adsorption of Cd^{2+} (C_0 , $3000 \text{ mg}\cdot\text{L}^{-1}$).

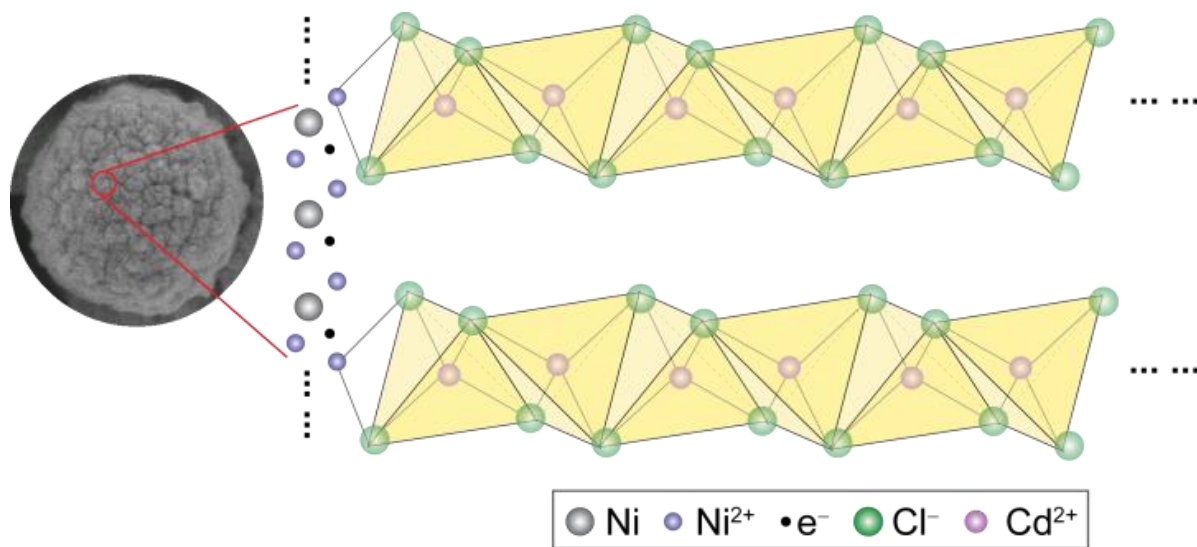


Fig. S12 Schematic drawing describing the proposed coordination bridging adsorption process of Cd²⁺ ions on the Ni microspheres.

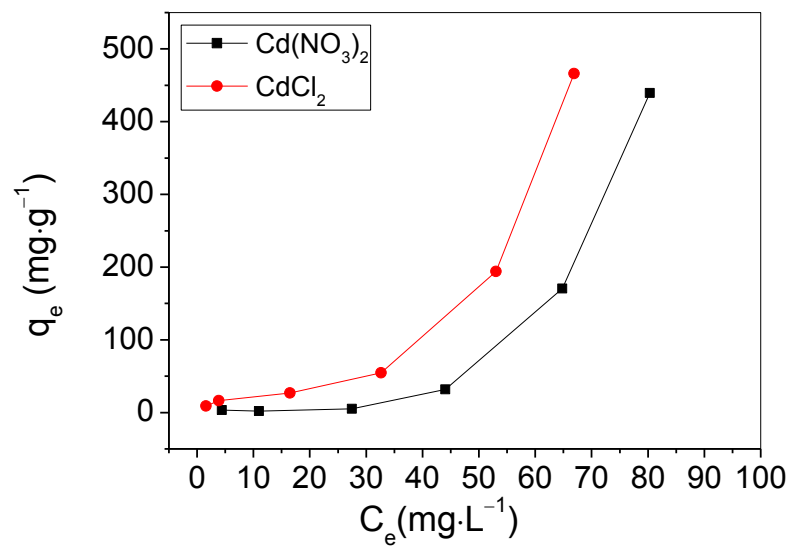


Fig. S13 The adsorption isotherm of Cd²⁺ ions on the Ni microspheres (0.5 g·L⁻¹) using Cd(NO₃)₂ instead of CdCl₂.

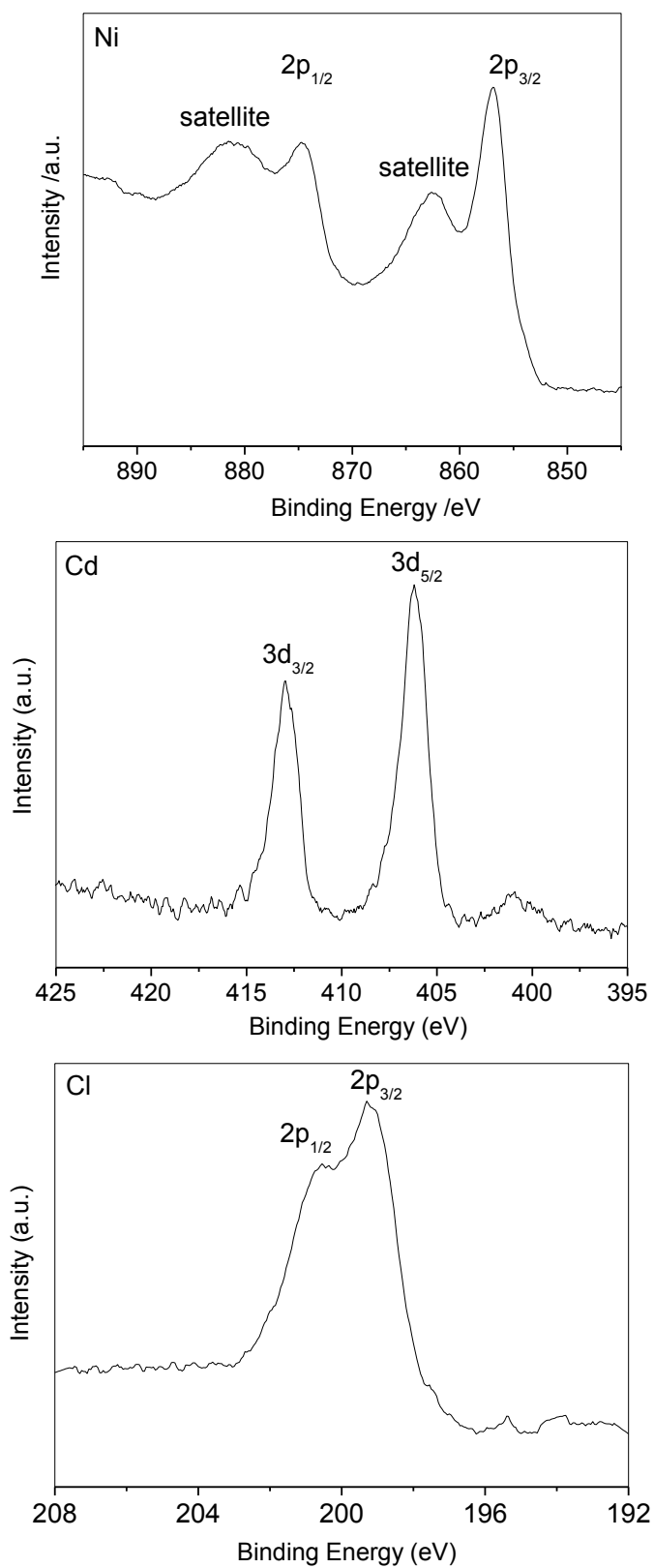


Fig. S14 Ni $2p_{1/2}$ and $2p_{3/2}$, Cd $3d_{3/2}$ and $3d_{5/2}$ and Cl $2p_{1/2}$ and $2p_{3/2}$ XPS spectra on the Ni microspheres after adsorption treatment.

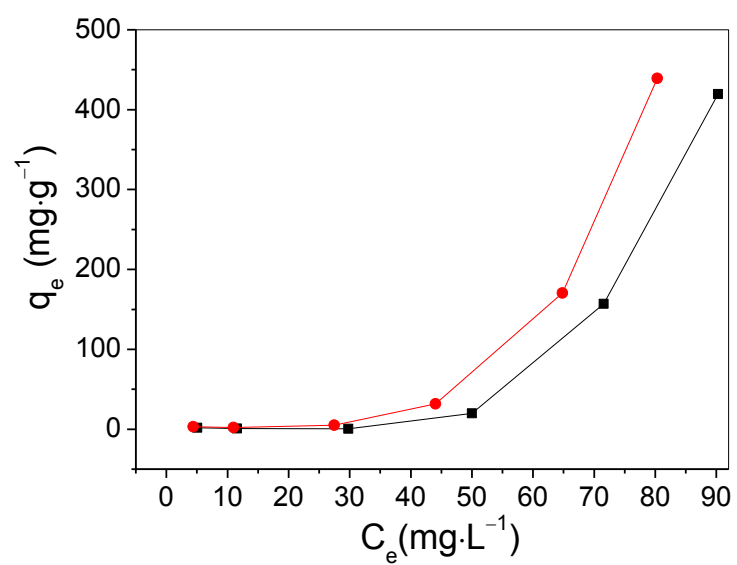


Fig. S15 The adsorption isotherm of Cd^{2+} ions on the Ni microspheres ($0.5 \text{ g}\cdot\text{L}^{-1}$, red line) and a non-uniform Ni material with a low density of Ni dots ($0.5 \text{ g}\cdot\text{L}^{-1}$, black line).

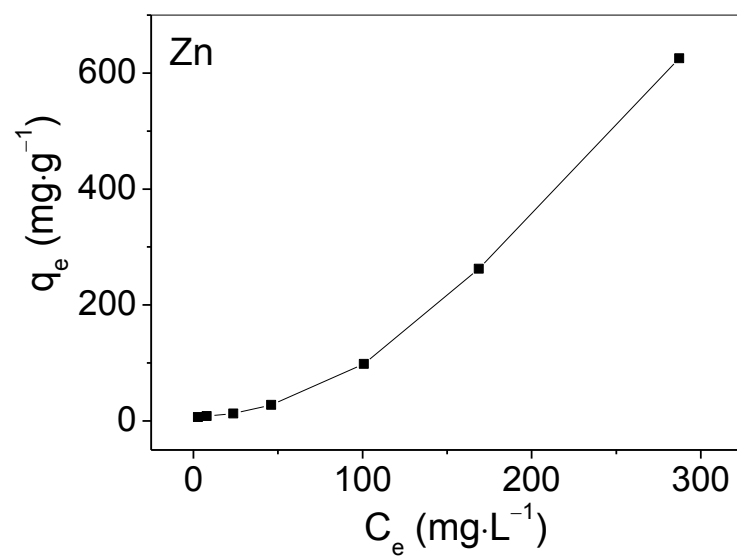


Fig. S16 The adsorption isotherm of Zn²⁺ ions on the Ni microspheres (0.5 g·L⁻¹) using ZnCl₂.

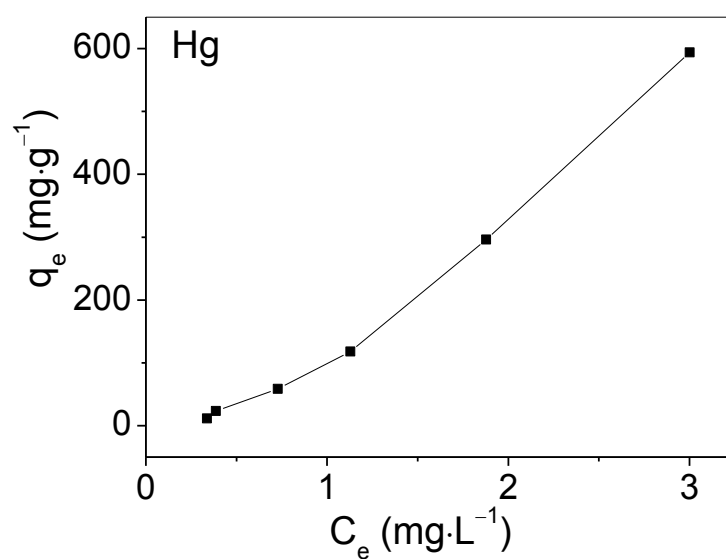


Fig. S17 The adsorption isotherm of Hg²⁺ ions on the Ni microspheres (0.5 g·L⁻¹) using HgCl₂.